

# An extension of the Generalized Actuator Disc Theory for aerodynamic analysis of the diffuser-augmented wind turbines

Liu, Yingyi

Interdisciplinary Graduate School of Engineering Science, Kyushu University

Yoshida, Shigeo

Research Institute for Applied Mechanics, Kyushu University

<https://hdl.handle.net/2324/4055203>

---

出版情報 : Energy. 93 (2), pp.1852-1859, 2015-12-15. Elsevier

バージョン :

権利関係 : Creative Commons Attribution NonCommercial NoDerivatives 4.0 International

1 **An extension of the Generalized Actuator Disc Theory for aerodynamic analysis**  
2 **of the diffuser-augmented wind turbines**

3 *Yingyi Liu<sup>1,\*</sup>, Shigeo Yoshida<sup>2</sup>*

4 <sup>1</sup>Interdisciplinary Graduate School of Engineering Science, Kyushu University, Kasuga, Fukuoka 816-8580, JAPAN

5 <sup>2</sup>Research Institute for Applied Mechanics, Kyushu University, Kasuga, Fukuoka 816-8580, JAPAN

6 -----  
7 **Abstract**

8  
9 The one-dimensional momentum theory is essential for understating the physical mechanism behind the phenomena of  
10 the DAWT (Diffuser-Augmented Wind Turbines). The present work tries to extend the existing GADT (Generalized  
11 Actuator Disc Theory) that proposed by Jamieson (2008). Firstly, the GADT is modified to include an effective diffuser  
12 efficiency, which is affected by the thrust loading or axial induction. Secondly, Glauert corrections to the DAWT system  
13 in the turbulent wake state are proposed, modelled by a linear and a quadratic approximation, respectively. Finally, for  
14 prediction of the axial velocity profile at rotor plane bearing various thrust loadings, an empirical model is established,  
15 which can be further used to predict the diffuser axial induction. In addition, the ‘cut-off point’ in Glauert correction and  
16 the ‘critical thrust loading’ in axial velocity profile prediction are newly defined to assist the analysis. All the above  
17 formulations have been compared and validated with Jamieson’s results and Hansen’s CFD data, justifying the  
18 effectiveness of the present model.

19  
20 *Keywords:* Momentum theory; Diffuser-augmented; effective diffuser efficiency; Glauert correction; velocity speed-up  
21 ratio

22 -----  
23 **1 Introduction**

24 It has long been pursued by the people around the world for energy extraction concepts with their  
25 efficiency as high as possible, among which the DAWT (Diffuser-Augmented Wind Turbines) can be  
26 viewed as one of those innovative technologies. With shrouding of the diffuser, DAWT may be

-----  
\* Corresponding author. Tel.: +81-080-8565-7934.  
E-mail address: liuyingyi@riam.kyushu-u.ac.jp

27 capable of exceeding the Betz limit (e. g. Oka et al. [1]), which has been usually considered as the  
28 limit of power performance coefficient of the bare wind turbines.

29 Many investigations have been done on DAWT technology on various aspects, which have been  
30 lasted over 50 years. Lilley and Rainbird [2] discovered that the increase in axial velocity and the  
31 reduction of blade tip losses might be the main factors for the additional power augmentation from a  
32 duct. Experimental studies later performed by Gilbert & Foreman ([3], [4]) and Igra [5], showing that  
33 power extraction beyond the Betz limit was possible. At the same time, Fletcher [6] attempted to  
34 develop a computational analysis method, based on coupling his momentum theory with the Blade  
35 Element Method. Dick [7] proved that for a mass concentrator similar to DAWT, the power coefficient  
36 of the system can be written as the product of a mass concentration coefficient and an extraction  
37 coefficient. Thereafter, the research on DAWT had been suspended for almost 20 years partly due to  
38 the technology had not been considered profitable relatively to conventional wind turbines at that  
39 moment. Relevant researches boomed again till the beginning of the 21<sup>st</sup> century, while Hansen et al.  
40 [8] simulated a diffuser which was made from deforming NACA0015 aerofoil by the CFD software  
41 *EllipSys*. Later, Van Bussel [9] first introduced the back pressure velocity ratio and showed that the  
42 power augmentation could be achieved by increasing the exit area ratio which leads to an under  
43 pressure at the nozzle. Jamieson ([10], [11], [12]) developed a generalized limit theory for the  
44 shrouded wind turbine through new formulations, aiming at its application to a DAWT BEM (Blade  
45 Element Method) code which was implemented in the wind turbine design software package *Bladed*.  
46 In short, until recently, the methodologies for investigating DAWT have mainly three branches, the  
47 computational (CFD) method, the theoretical (empirical) method and the experimental method, which  
48 have been all performed in the history.

49 As known by all, for the design purpose, it is necessary to develop a fast and accurate method,  
50 in order to reduce the economic cost and the labour force. Therefore, we are always trying not to

51 depend on experiment or CFD too much. The theoretical method provides a best solution taking into  
52 account both the cost and the efficiency, as long as the accuracy is guaranteed. The theoretical model  
53 for DAWT has evolved into several versions based on the understanding of the physical mechanism  
54 for the augmentation, among which Jamieson's formulation looks more comprehensive, since it has  
55 already been designed to cover the previous models at the beginning. Other's experimental results and  
56 Hansen's CFD computational results supply an extensive database for the possible validations on  
57 various aspects of the theoretical model. Particularly, for the one-dimensional momentum theory  
58 discussed in the following sections in which the detailed form of rotor is not considered too much, it  
59 is worth to note that the Hansen's data, which was obtained by implementing the Actuator Disc Model  
60 in the CFD simulation, gives a sound validation benchmark for this specific issue.

61 The motivation of the present work comes from the interest in trying to consummate the existing  
62 Jamieson's theoretical model, by bringing about more light into it through some necessary effort. In  
63 the following parts, the paper discusses the links between Jamieson's theory and the previous classical  
64 theory, compares the approximation methods for the effective energy diffuser efficiency of the DAWT  
65 system, improves the Glauert correction for the thrust coefficient in the turbulent wake state, and  
66 proposes an empirical model for prediction of the axial velocity profile and the diffuser axial induction  
67 distribution at the rotor plane.

## 68 **2 Fundamental methodologies for the diffuser-augmented wind turbines**

### 69 *2.1 The Generalized Actuator Disc Theory*

70 The Generalized Actuator Disc Theory (GADT) was first proposed by Jamieson [10], and then  
71 discussed in Jamieson [11] and Jamieson [12]. It extends the existing ADT (Actuator Disc Theory) to  
72 a more general case of a shrouded wind turbine, through the introduction of a new axial induction  
73 factor  $a_0$  which accounts for the geometry of the given diffuser. As shown in Fig. 1, for the generalized  
74 flow in the upstream side of the extracted plane, application of Bernoulli's equation leads to

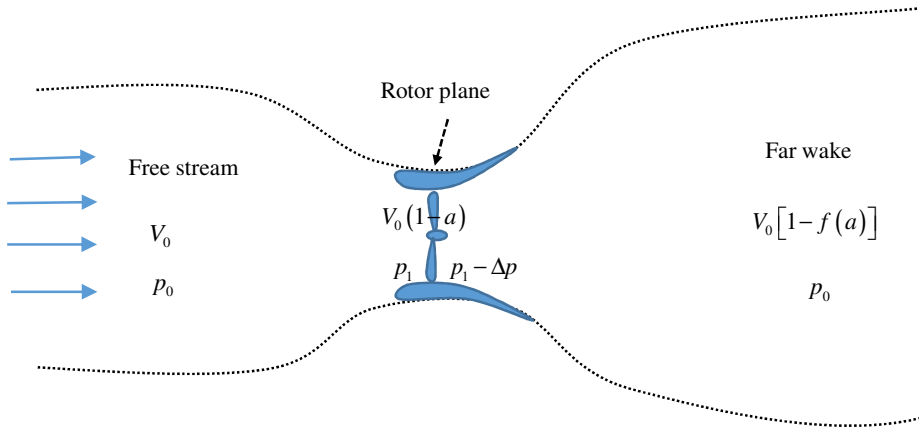
75 
$$p_0 + \frac{1}{2} \rho V_0^2 = p_1 + \frac{1}{2} \rho V_0^2 (1-a)^2, \quad (1)$$

76 and for the downstream flow, similarly

77 
$$p_1 - \Delta p + \frac{1}{2} \rho V_0^2 (1-a)^2 = p_0 + \frac{1}{2} \rho V_0^2 [1-f(a)]^2 \quad (2)$$

78 where  $f(a)$  is assumed as the axial induction in the far wake. On the other hand, consider the relation  
79 between the pressure variations at any plane with the thrust coefficient

80 
$$C_{T,d} = \frac{2\Delta p}{\rho V_0^2}. \quad (3)$$



81

82 Fig. 1 Sketch of the diffuser-augmented wind turbine system

83 Combination of Eqs. (1) ~ (3) leads to the relation of the thrust coefficient with the axial induction in  
84 the far wake

85 
$$C_{T,d} = f(a)[2-f(a)]. \quad (4)$$

86 The function  $f(a)$  is unknown, but restricted to the following three conditions: (1) in the absence of  
87 energy extraction,  $a = a_0$ , and  $f(a) = 0$ ; (2) when the flow is fully blocked,  $a = 1$ , and  $C_{T,d} = 0$ ; (3) in  
88 the presence of the rotor, since energy is extracted out from the system, the velocity in the far wake  
89 must be less than the ambient, i.e.,  $f(a) > 0$  for  $a > a_0$ . Solution of Eq. (4) therefore becomes

90 
$$f(a) = \frac{2(a - a_0)}{1 - a_0}, \quad (5)$$

91 and

92 
$$C_{T,d} = \frac{4(a - a_0)(1 - a)}{(1 - a_0)^2}. \quad (6)$$

93 Since the power coefficient  $C_{P,d}$  has a relation with  $C_{T,d}$

94 
$$C_{P,d} = (1 - a)C_{T,d}, \quad (7)$$

95 We have

96 
$$C_{P,d} = \frac{4(a - a_0)(1 - a)^2}{(1 - a_0)^2}. \quad (8)$$

97 Differentiating Eq. (8) with respect to  $a$  determines the maximum power coefficient

98 
$$C_{P,d}^{\max} = \frac{8}{9}(1 - a_m) \quad (9)$$

99 at  $a = a_m$  where

100 
$$a_m = \frac{1 + 2a_0}{3}. \quad (10)$$

101 The corresponding thrust coefficient matched with maximum energy extraction (optimal rotor  
102 loading) is

103 
$$C_{T,d}^{\text{opt}} = \frac{8}{9}. \quad (11)$$

## 104 2.2 The classical theory for shrouded wind turbines

105 The classical DAWT theory has been developed through a much longer time history. Derivation  
106 of the formulation in detail can be found in many previous works (Fletcher [6]; Hansen et al. [8]; Rio  
107 Vaz et al. [13]). In this theory, the momentum equation keeps a consistent form with the classical

108 theory without diffuser. It introduces the diffuser velocity speed-up ratio  $\gamma$  as its key part to account  
 109 for the shrouding effect. In order to distinguish from the definition of  $a$  that is used by Jamieson's  
 110 theory, herein we use  $b$  to express the axial induction factor. The critical difference between them is  
 111 that  $a$  represents the induction at the rotor plane, whereas  $b$  represents the induction at the downstream  
 112 far wake. The velocity speed-up ratio  $\varepsilon$  is defined as the ratio of the flow velocity at the rotor plane to  
 113 the free-stream velocity

$$114 \quad \varepsilon = \frac{V_1}{V_0}, \quad (12)$$

115 which can be also written in an alternative way as the product of diffuser augmentation and loss of  
 116 rotor blockage

$$117 \quad \varepsilon = \gamma(1-b). \quad (13)$$

118 The thrust coefficient and power coefficient are

$$119 \quad C_{T,d} = 4b(1-b) \quad (14)$$

120 and

$$121 \quad C_{P,d} = \gamma 4b(1-b)^2, \quad (15)$$

122 respectively. Notice that Eqs. (14) and (15) also hold for the bare-rotor thrust coefficient  $C_{T,b}$  and the  
 123 power coefficient  $C_{P,b}$  when  $\gamma=1$ . In addition, from Eqs. (14) and (15) we obtain

$$124 \quad C_{P,d} = \varepsilon C_{T,d}. \quad (16)$$

### 125 *2.3 Finding links between the two momentum theories*

126 In the classical DAWT theory, it is well-known that the downstream velocity in the far wake is

$$127 \quad V_2 = (1-2b)V_0. \quad (17)$$

128 Comparing with Jamieson's theory it can be found that  $b$  is equivalent to the half of induction in the  
129 far wake

$$130 \quad b = \frac{a - a_0}{1 - a_0}, \quad (18)$$

131 which shows that  $b$  involves the effect of diffuser.

132 On the other hand, according to the definition of Hansen et al. [8] and Jamieson [11], the diffuser  
133 velocity speed-up ratio can be expressed by

$$134 \quad \gamma = 1 - a_0. \quad (19)$$

135 Therefore, considering Eqs. (13), (18) and (19), we obtain

$$136 \quad \varepsilon = (1 - a_0) \left( 1 - \frac{a - a_0}{1 - a_0} \right) = 1 - a. \quad (20)$$

137 Since  $1 - a$  is exactly the ratio of rotor-plane flow velocity to the free-stream velocity that is defined  
138 in Jamieson's theory, which coincides with the definition of  $\varepsilon$  defined in the classical theory with  
139 diffuser, Eq. (20) proves the consistence between the two theories.

140 As pointed out by Hansen et al. [8], the relative increase in the power coefficient for a diffuser-  
141 augmented wind turbine is proportional to the ratio of mass flow through the same rotor with and  
142 without the diffuser

$$143 \quad \frac{C_{P,d}}{C_{P,b}} = \frac{\dot{m}_d}{\dot{m}_b} = \frac{\varepsilon}{1 - b}. \quad (21)$$

144 Combination of Eqs. (13), (19) and (21) leads to

$$145 \quad \frac{C_{P,d}}{C_{P,b}} = \frac{\dot{m}_d}{\dot{m}_b} = 1 - a_0. \quad (22)$$



146 This result shows the ratio of power coefficient between the shrouded and the non-shrouded turbine  
 147 under the same thrust loading depends on the diffuser axial induction factor  $a_0$ , which relies on the  
 148 given geometry of the diffuser.

### 149 **3 Effective diffuser efficiency for evaluation of the turbine performance**

150 The diffuser is not ideal if its maximum power coefficient does not occur at optimal rotor loading.  
 151 This imperfection can be measured by a variable function which is called ‘effective diffuser  
 152 efficiency’, approximating how closely the efficiency of the present diffuser at current status  
 153 approaches the optimal performance of its initial design (Jamieson [11]). Consider a real diffuser  
 154 system under non-optimum loading, and assume the effective diffuser efficiency to be a function of  
 155 the axial induction factor

$$156 \quad \eta(a) = \frac{C_{T,d}(a)}{C_{T,d}^{opt}}, \quad (23)$$

157 the diffuser axial induction is actually not  $a_0$ , but  $a_0\eta(a)$ . The expressions for the thrust coefficient and  
 158 the power coefficient therefore need to be improved by a slight modification on the axial induction  
 159 factor, which can be re-expressed as

$$160 \quad C_{T,d} = \frac{4[a - a_0\eta(a)](1-a)}{(1-a_0)^2}, \quad (24)$$

161 and

$$162 \quad C_{P,d} = \frac{4[a - a_0\eta(a)](1-a)^2}{(1-a_0)^2}. \quad (25)$$

163 It should be noticed that the function  $\eta(a)$  here is not always constant with respect to  $a$ , since it has  
 164 been pointed out by Jamieson [11] that the constant effective diffuser efficiency is strictly valid only

165 at the critical condition where  $C_{P,d}$  is maximum. Additionally, the ratio of mass flow between the  
 166 shrouded and the non-shrouded turbine can also be re-expressed as

$$167 \quad \frac{C_{P,d}}{C_{P,b}} = \frac{\dot{m}_d}{\dot{m}_b} = (1 - a_0) \eta(a). \quad (26)$$

168 Eq. (26) is very useful for calculating the effective diffuser efficiency under different thrust loading.

169 In the meantime, solution for  $a$  from Eq. (24) is

$$170 \quad a = \frac{1}{2} \left\{ [1 + a_0 \eta(a)] - \sqrt{[1 - a_0 \eta(a)]^2 - (1 - a_0)^2 C_{T,d}} \right\}, \quad (27)$$

171 which can be used to calculate  $a$  if the relationship between  $\eta(a)$  and  $C_{T,d}$  is known.

172 However, the exact form of the variable function  $\eta(a)$  is usually unknown beforehand. Jamieson  
 173 [11] proposed a linear approximation in  $a$  which can be written as

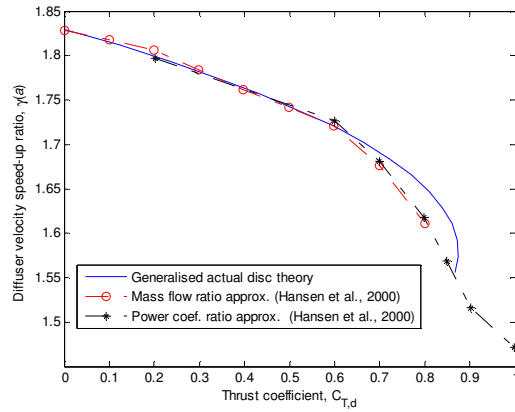
$$174 \quad \eta(a) = \frac{a(1 - \eta_{pmax}) - a_m + a_0 \eta_{pmax}}{a_0 - a_m}, \quad (28)$$

175 where  $a_m$  is modified into

$$176 \quad a_m = \frac{1 + 2a_0 \eta_{pmax}}{3} \quad (29)$$

177 and  $\eta_{pmax} = \eta(a_{pmax})$  represents the effective diffuser efficiency at power maximum point, which is  
 178 also defined as the ‘diffuser efficiency’ in Jamieson’s formulation.

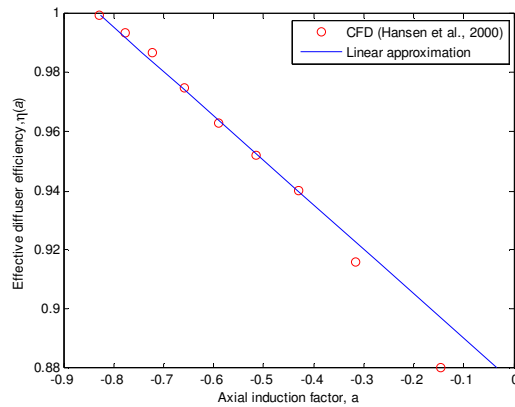
179 Hansen’s CFD results (Ref. [8]) provide a good source for verifying the above theory. In his  
 180 work, the diffuser was made by deforming a NACA0015 airfoil. According to his quotation, for zero  
 181 thrust loading, the ratio of the flow velocity at the rotor plane to the free-stream velocity is  $\gamma = 1.83$ ,  
 182 which means in the rotor absent state,  $a_0 = -0.83$ . Besides, its maximum power coefficient occurs at  
 183  $C_{T,d} = 0.8$  indicating that the diffuser efficiency is 0.9 based on Eq. (23), as pointed out by Jamieson  
 184 [11].



185

186 Fig. 2 Verification of theoretical results with CFD for the diffuser velocity speed-up ratio

187 Hansen et al. [8] supplies the  $C_P - C_T$  curve (including data for both shrouded rotor and non-  
 188 shrouded rotor) and the  $\eta - C_T$  curve, which can both be used to calculate the diffuser velocity speed-  
 189 up ratio and further the effective diffuser efficiency, through Eq. (26). Theoretical prediction of  $\gamma - C_T$   
 190 relation by Eq. (24) coincides very well with that obtained from the CFD data when  $C_T$  is less than  
 191 0.6, as shown in Fig. 2, which validates Eq. (24) when  $C_T$  is small. The inconsistency for  $C_T$  above  
 192 0.6 is caused by the turbulent wake state, where usually a Glauert-like correction should be used to  
 193 eliminate the discrepancy. In the meantime, Fig. 2 confirms the validity of Eq. (23), since the  $\gamma - C_T$   
 194 relations obtained from the mass flow ratio approximation and the power coefficient approximation  
 195 seem to be equivalent.



196

197

Fig. 3 Linear approximation for the effective diffuser efficiency

198

199

200

Fig. 3 compares the linear approximation based on Eq. (28) with the CFD data for prediction of the  $\eta - a$  relation. It can be observed that the linear formula provides a good approximation especially for the range  $\eta > 0.94$ .

201

#### 4 Extended Glauert correction to the DAWTs in turbulent wake state

202

203

204

205

206

207

208

209

210

211

Similar to the ADT for the bare rotor in open flow, the GADT for the shrouded rotor in constrained flow needs a Glauert correction as well when the rotor approaches the turbulent wake state. In Section 3, the discrepancy between the theoretical and the computational results is found at about  $C_T = 0.6$ . In the extreme case that the DAWT system works always at optimal status for all the thrust loading, substituting Eq. (18) into Eq. (14) leads to the Eq. (6), which means the two formulations are equivalent. The half far-wake induction  $b$  defined by Eq. (18) thus can be used as a basic variable for Glauert correction, as that has been done to  $a$  in the open flow ADT. Consider the general case when there exists an effective diffuser efficiency for the DAWT system, substitution of the generalized version of Eq. (18) into Eq. (14) does not certainly lead to Eq. (24). The resulting expression of the thrust coefficient is therefore

212

$$C_{T,d} = \frac{4[a - a_0\eta(a)]\{1 - a + [\eta(a) - 1]a_0\}}{(1 - a_0)^2}. \quad (30)$$

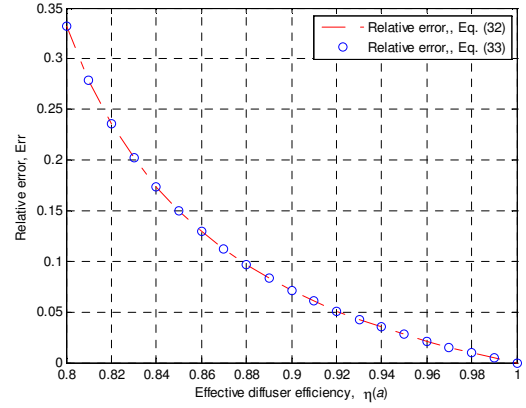
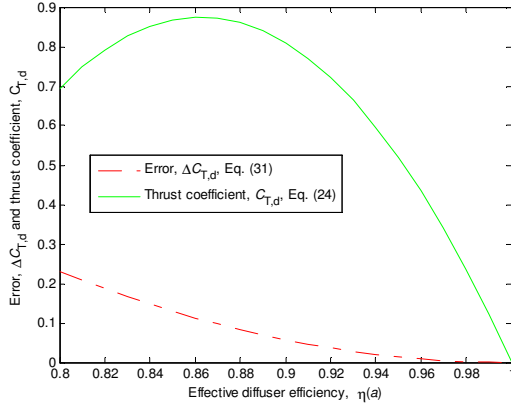
213

214

Subtracting Eq. (24) from Eq. (30) and taking into consideration the linear  $\eta - a$  relation Eq. (28), difference between the two expressions can be written as

215

$$\Delta C_{T,d} = -\frac{4[1 - \eta(a)]^2(1 - a_0\eta_{pmax})a_0}{3(1 - \eta_{pmax})(1 - a_0)^2}. \quad (31)$$



216

217

(a) absolute error

(b) relative error

218

Fig. 4 Error estimation for the substitution of Eq.(30) for Eq.(24)

219 Ratio of Eq. (31) to Eq. (24) gives the relative error

$$220 \quad Err = \left| \frac{\Delta C_{T,d}}{C_{T,d}} \right| = -\frac{1}{3} \frac{[1-\eta(a)]^2 (1-a_0 \eta_{pmax}) a_0}{(1-\eta_{pmax}) [a - a_0 \eta(a)] (1-a)}, \quad (32)$$

221 which could also be given directly based on the difference between Eq. (30) and Eq. (24)

$$222 \quad Err = \left| \frac{\Delta C_{T,d}}{C_{T,d}} \right| = \frac{[\eta(a) - 1] a_0}{1-a}. \quad (33)$$

223 Fig. 4 shows the error estimation of employing the half far-wake induction  $b$  as the variable in  
 224 the thrust coefficient formulation Eq. (14), as that is done in open flow condition. It is evident from  
 225 Fig. 4(a) that the absolute error for the thrust coefficient decreases with the increase of the effective  
 226 diffuser efficiency. Fig. 4(b) is the local magnification of the relative error when  $\eta$  becomes large,  
 227 from which it is seen that the relative error is less than 5% for the region  $\eta > \eta_c = 0.937$ , where we  
 228 define  $\eta_c$  as the “cut-off point” between the ordinary thrust coefficient equation and the Glauert  
 229 correction. Through Eq. (28) and the generalized version of Eq. (18), the corresponding values of the  
 230 axial induction and the half far-wake induction at the cut-off point can be calculated out as  $a_c = -0.412$

231 and  $b_c = 0.2$ . Similar process can be performed to the values at the power maximum point. The results  
 232 are listed in Table 1.

233 Table 1. Calculated values at the two key points

	$a$	$b$	$\eta$	$C_{T,d}$	$C_{P,d}$
cut-off point	-0.4118	0.2000	0.9371	0.6172	0.8714
maximum power point	-0.1788	0.3105	0.9000	0.8000	0.9431

234  
 235 For the Glauert correction, Jamieson [12] gives the formula, which is also used in the DNV GL's  
 236 commercial BEM software *Bladed*:

$$237 \quad C_{T,d}(a) = \begin{cases} \frac{4[a - a_0\eta(a)](1-a)}{(1-a_0)^2} \\ \text{for } 0 \leq a \leq a_0 + 0.3539(1-a_0) \\ 0.6 + 0.61 \left[ \frac{a - a_0\eta(a)}{1-a_0} \right] + 0.79 \left[ \frac{a - a_0\eta(a)}{1-a_0} \right]^2 \\ \text{for } a_0 + 0.3539(1-a_0) < a \leq 1 \end{cases}, \quad (34)$$

238 where the result is shown in Fig. 5. Since the two curves has been detached from each other, it is  
 239 necessary to make them connected. The detachment of the two curves is partly due to the cut-off point  
 240 occurring at  $b_c = 0.3539$ , which can be obviously seen in Eq. (34). Therefore it is better to move the  
 241 cut-off point forward. We choose  $b_c = 0.2$  in our following formulations.

242 Generally, the ‘artificial’ Glauert correction can be made by a polynomial function with any order  
 243 for the dependent variable, as long as the accuracy is satisfactory within prescribed tolerance range.  
 244 Although, the linear form is the simplest, it may be very helpful in practical engineering issues. We  
 245 choose the values at the optimal point  $(b_{pmax}, C_{T,d}^{pmax})$  and the cut-off point  $(b_c, C_{T,d}^c)$  to determine the  
 246 linear equation of the straight line

247 
$$C_{T,d}(b) - C_{T,d}^{pmax} = \frac{C_{T,d}^{pmax} - C_{T,d}^c}{b_{pmax} - b_c} (b - b_{pmax}). \quad (35)$$

248 where  $b_{pmax} = \frac{a_{pmax} - a_0 \eta_{pmax}}{1 - a_0}$  and  $b_c = \frac{a_c - a_0 \eta_c}{1 - a_0}$ . In the present case, the equation finally leads to the

249 linear Glauert correction

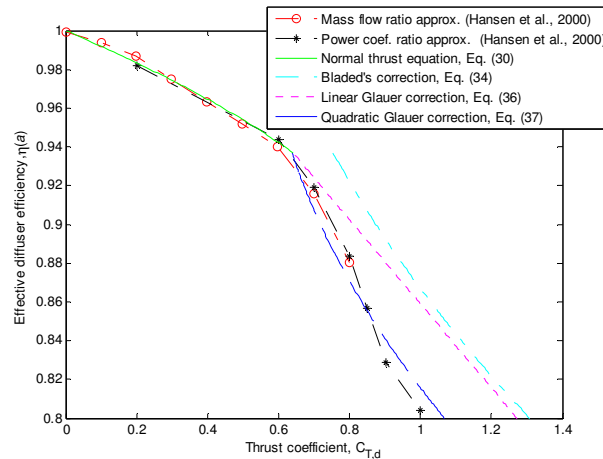
250 
$$C_{T,d}(a) = \begin{cases} 4 \left[ \frac{a - a_0 \eta(a)}{1 - a_0} \right] \left[ 1 - \frac{a - a_0 \eta(a)}{1 - a_0} \right] \\ \text{for } a_0 \leq a \leq a_0 + 0.2(1 - a_0) \\ 0.3504 + 1.4482 \left[ \frac{a - a_0 \eta(a)}{1 - a_0} \right] \\ \text{for } a_0 + 0.2(1 - a_0) < a \leq 1 \end{cases}. \quad (36)$$

251 A second alternative choice is to apply quadratic polynomials for the thrust equation in the  
 252 turbulent state. The method of Marshall (2005) can be used, which applies the continuity condition  
 253 for the function value and the function derivative value at the cut-off point, and the continuity  
 254 condition for the function value at the optimal point. However, Marshall (2005)'s method will lead to  
 255 an apparent gap between the resulting Glauert correction curve and Hansen's CFD data especially  
 256 when  $C_{T,d}$  is large. Here we give one of the quadratic polynomial that better fit the CFD data as below

257 
$$C_{T,d}(a) = \begin{cases} 4 \left[ \frac{a - a_0 \eta(a)}{1 - a_0} \right] \left[ 1 - \frac{a - a_0 \eta(a)}{1 - a_0} \right] \\ \text{for } a_0 \leq a \leq a_0 + 0.2(1 - a_0) \\ 0.5632 + 0.1815 \left[ \frac{a - a_0 \eta(a)}{1 - a_0} \right] \\ + 0.9602 \left[ \frac{a - a_0 \eta(a)}{1 - a_0} \right]^2 \\ \text{for } a_0 + 0.2(1 - a_0) < a \leq 1 \end{cases}. \quad (37)$$

258 Fig. 5 shows comparison of the different schemes for the Glauert correction of the DAWT system.  
 259 The form of Eq. (30) for the normal thrust equation agrees well with the scattered CFD data in the  
 260 region of  $\eta \geq \eta_c$ . The error for the substitution of Eq. (24) is acceptable, as discussed in Fig. 4. In the

261 region of  $\eta < \eta_c$ , *Bladed's* Glauert correction seems to have a bit larger distance to the scattered points,  
 262 while the linear Glauert correction and the quadratic Glauert correction proposed in this paper behaves  
 263 better.



264

265 Fig. 5 Comparison of various schemes of Glauert correction

266 **5 Prediction of the axial velocity profile at the rotor plane**

267 In the GADT argued above, a physical parameter, i.e., the diffuser axial induction  $a_0$ , which is  
 268 also related to the velocity speed-up ratio  $\varepsilon$  at the rotor plane, plays the most important role. Through  
 269 the introduction of this parameter, all the mathematical modelling becomes possible. Measurement or  
 270 computation of the parameters  $a_0$  or  $\varepsilon$  needs a large amount of labour force and economical expense.  
 271 It is better to develop an empirical method instead that can predict these parameters accurately, with  
 272 sufficient validation.

273 Normally, to determine the diffuser axial induction  $a_0$ , the wind velocity profile at the rotor plane  
 274 needs to be known in advance. This comes to the velocity speed-up ratio  $\varepsilon$ , since it is defined as the  
 275 augmentation of flow velocity at the rotor plane. As revealed by Eq. (13), the velocity speed-up ratio  
 276 under an arbitrary thrust loading can be decomposed into two factors, the diffuser velocity speed-up  
 277 ratio  $\gamma$  and the factor involving rotor axial induction  $(1 - b)$ . Particularly, in the extreme case of zero



278 thrust loading, the factor  $(1 - b)$  vanishes, leading to  $\varepsilon = \gamma = 1 - a_0$ , which indicates the diffuser axial  
 279 induction  $a_0$  can be determined, as long as the distribution of the velocity ratio  $\varepsilon$ , which is also named  
 280 as the axial velocity profile, is provided.

281 Due to the effect of diffuser, the axial velocity has an initial profile under zero thrust loading,  
 282 which is speeded up most obviously in the region close to the diffuser wall, and decreases to the centre  
 283 of the rotor disc. With the action of thrust force on the disc, the initial speeding up is counteracted by  
 284 the axial induction from the rotor, and becomes increasingly weaker and weaker, until it is completely  
 285 cancelled out and reversed by the rotor induction. Based on this mechanism, taking into consideration  
 286 the similar tip-loss model in the BEM methodology, we suppose the following formula for the axial  
 287 velocity profile with respect to the thrust loading and the radial location:

$$288 \quad \varepsilon = p - \frac{2}{\pi} \cos^{-1} (e^{-f}) \quad (38)$$

289 and

$$290 \quad f = \frac{g}{2} \frac{R - r}{R}, \quad (39)$$

291 where  $g$  and  $p$  are two parameters that can be determined by linear approximations

$$292 \quad g = \left( \frac{g_1 - g_0}{C_{T,d}^1 - C_{T,d}^0} \right) (C_{T,d} - C_{T,d}^0) + g_0, \quad (40)$$

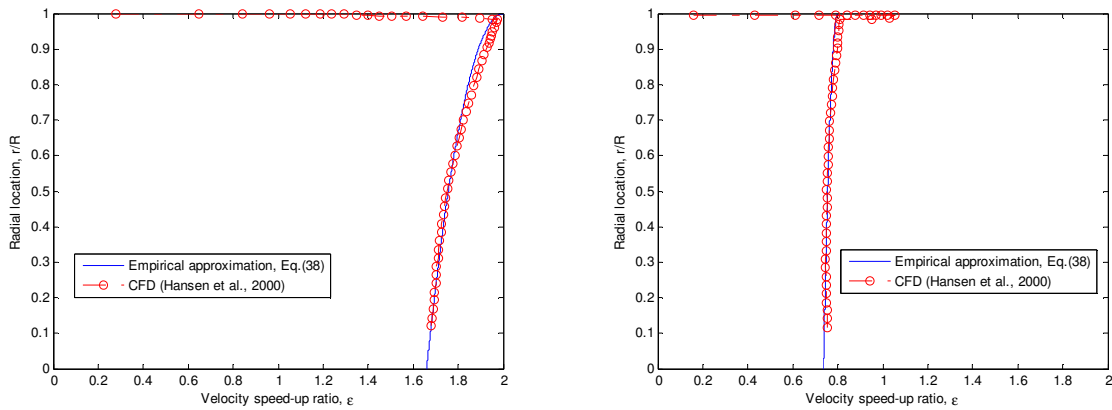
293 and

$$294 \quad p = \left( \frac{p_1 - p_0}{C_{T,d}^1 - C_{T,d}^0} \right) (C_{T,d} - C_{T,d}^0) + p_0, \quad (41)$$

295 where the subscript and the superscript '0' denotes the situation under zero thrust loading, and '1'  
 296 denotes the situation under full thrust loading  $C_{T,d} = 1.0$ . The quantities  $g$  and  $p$  are trying to describe  
 297 the curvature and the maximum value of the velocity profile, respectively, which are induced by the

298 combined action from the diffuser augmentation and the thrust loading. The value of  $g$  and  $p$  in these  
 299 two subscripts can be determined by the computed profile by CFD simulation under these two  
 300 conditions.

301 In the numerical example of Hansen et al. [8], the data of two axial velocity profiles computed  
 302 by CFD are provided. Through some simple test, we determine the parameters as  $g_0 = 0.3$ ,  $g_1 = 0.01$ ,  
 303  $p_0 = 2$  and  $p_1 = 0.8$ . Comparison for the approximated and the computed profiles is shown in Fig. 6.  
 304 The two results agree very well with each other, which verifies that the present empirical model is  
 305 quite helpful for prediction of the axial velocity profile under different thrust loadings.



306

(a)  $C_{T,d} = 0.0$

(b)  $C_{T,d} = 1.0$

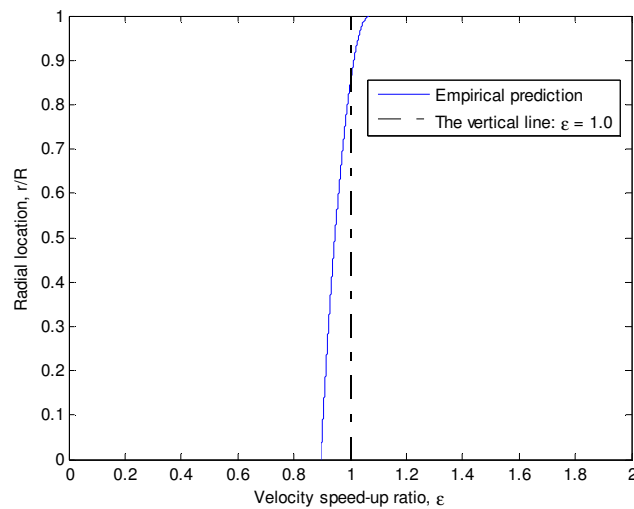
307

308 Fig. 6 Comparison of axial velocity profiles computed by the empirical model and CFD

309 The predicted axial velocity profile is essential to the determination of the velocity speed-up ratio  
 310 and the diffuser axial induction at different radial locations. It provides important information for the  
 311 input of the Generalized Blade Element Method (GBEM), in which the diffuser axial induction is  
 312 required to be known at different radial locations beforehand. To calculate the averaged value of the  
 313 diffuser velocity speed-up ratio  $\gamma$  and the diffuser axial induction  $a_0$ , we just need to simply compute  
 314 the area bounded by the profile curve and the lines of  $r/R = 0$  and  $\varepsilon = 0$  in the condition  $C_{T,d} = 0.0$ ,  
 315 and then divided by one. Numerical integration of the surrounded area in Fig. 6(a) gives the

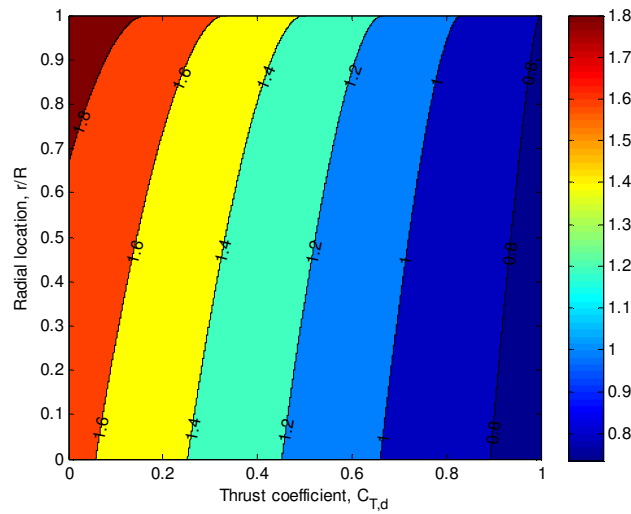
316 approximated result  $\gamma = 1.78$ , thus  $a_0 = 1 - \gamma = -0.78$ . Comparing with the value given in Hansen et al.  
 317 [8], i.e.,  $a_0 = -0.83$ , there is an absolute error 0.05 or a relative error 6.02%.

318 Since  $\varepsilon > 1.0$  when  $C_{T,d} = 0.0$ , and  $\varepsilon < 1.0$  when  $C_{T,d} = 1.0$ , there must be a value of  $C_{T,d}$  under  
 319 which the velocity speed-up ratio  $\varepsilon$  is equal to unity. As inferred from Eq. (20), at this loading  
 320 condition, the axial induction should be zero, which implies that the augmentation effect of the diffuser  
 321 is completely cancelled out by the induction effect of the rotor. Therefore, we define this loading as  
 322 ‘zero-induction thrust loading’, also as ‘critical thrust loading’. Fig. 7 shows prediction of the axial  
 323 velocity profile under the critical thrust loading  $C_{T,d}^{cr}$ . Again, through the similar technique, integration  
 324 gives the averaged value of the velocity speed-up ratio  $\varepsilon = 0.953$ , which approximately approaches  
 325 unity, with an absolute error 0.047 or a relative error 4.7%.



326

327 Fig. 7 Prediction of the axial velocity profiles under the critical thrust loading



328

329 Fig. 8 Distribution of the velocity speed-up ratio at various thrust loadings and radial locations

330 Fig. 8 shows the contour plot of the velocity speed-up ratio under various thrust loadings and at  
 331 different radial locations. It can be evidently seen that, the smaller the thrust loading is and the larger  
 332 the radial distance is, the larger the velocity speed-up ratio will be. The largest velocity speed-up ratio  
 333 occurs in the region near the point  $C_{T,d} = 0.0$  and  $r/R = 1.0$ , and the smallest velocity speed-up ratio  
 334 occurs at the region near the point  $C_{T,d} = 1.0$  and  $r/R = 0.0$ . The visual result is reasonable by  
 335 contrasting to the CFD profile given in Hansen et al. [8].

336 **Conclusions**

337 The GADT that first brought forth by Jamieson ([10], [11]) helps a lot in revealing the physical  
 338 mechanism for the diffuser-augmented wind turbine behind the phenomena. It can be better  
 339 understood through taking into consideration simultaneously the classical theory for shrouded wind  
 340 turbine. The present work tries to dig more deeply in the GADT, including the following aspects:

- 341 (1) Links between the GADT and the classical DAWT theory has been argued, especially the  
 342 relation between the axial induction and the velocity speed-up ratio.

343 (2) Jamieson's linear approximation formulation for the effective diffuser efficiency has been  
344 compared with Hansen's CFD data, showing that it works pretty well especially in the high diffuser  
345 efficiency range.

346 (3) Glauert corrections for the DAWT are studied. A linear and a quadratic approximation  
347 formulae have been proposed. Validation is given by comparing with Jamieson's formula and  
348 Hansen's CFD data.

349 (4) The GADT is further extended to include approximation of the axial velocity profile by  
350 establishing an empirical model, which is essential to the prediction of the diffuser axial induction.  
351 Comparison between the CFD results justifies the effectiveness of the present model.

352 It should be noticed that at the current stage, the above GADT is still necessary to be applied  
353 with the assist of the CFD method, particularly for the determination of its several important  
354 parameters. In addition, the empirical model for predicting the axial velocity profile still cannot  
355 explain the small gap close to the region between the blade tip and the boundary layer of the diffuser  
356 wall, which should be further improved as a future work.

### 357 **Acknowledgements**

358 All the authors gratefully appreciate the valuable discussions with Prof. Jamieson in the past  
359 research. The first author gratefully acknowledges the financial support provided by the MEXT  
360 Scholarship (Grant No. 123471) from Japanese Government during the three-year PhD research.

### 361 **References**

- 362 [1] N. Oka, M. Furukawa, K. Yamada, K. Kawamitsu, K. Kido, A. Oka, Aerodynamic Design Optimization of  
363 Wind-lens Turbine. EWEA 2014, Barcelona, Spain.
- 364 [2] W.J. Rainbird, G.M. Lilley, A Preliminary Report on the Design and Performance of a Ducted Windmill.  
365 (Report 102), College of Aeronautics Cranfield, 1956.

- 366 [3] B.L. Gilbert, K.M. Foreman, Fluid Dynamics of Diffuser-Augmented Wind Turbines. *Journal of Energy*  
367 1978; 2(6): 368 – 374.
- 368 [4] B.L. Gilbert, K.M. Foreman, Experimental Demonstration of the Diffuser-Augmented Wind Turbine  
369 Concept. *Journal of Energy* 1979; 3(4): 235 – 240.
- 370 [5] O. Igra, Research and development for shrouded wind turbines. *Energy Convers Manage* 1981; 21:13–48.
- 371 [6] C.A. Fletcher, Computational analysis of diffuser-augmented wind turbines. *Energy Convers Manage* 1981;  
372 21:175–83.
- 373 [7] E. Dick, Momentum analysis of wind energy concentrator systems. *Energy Convers Manage* 1984; 24:19–  
374 25.
- 375 [8] M.O.L. Hansen, N.N. Sorensen, R.G.J. Flay, Effect of placing a diffuser around a wind turbine. *Wind Energy*  
376 2000; 3:207–213.
- 377 [9] G.J.W. Van Bussel, The science of making more torque from wind: diffuser experiments and theory  
378 revisited. *Journal of Physics: Conference Series* 2007; 75(1): 1–12.
- 379 [10] P. Jamieson, Generalized limits for energy extraction in a linear constant velocity flow field. *Wind Energy*  
380 2008; 11: 445 – 457.
- 381 [11] P. Jamieson, Beating Betz - Energy Extraction Limits in a Uniform Flow Field. EWEC 2008, Brussels,  
382 Belgium.
- 383 [12] P. Jamieson, *Innovation in wind turbine design*. John Wiley & Sons, 2011.
- 384 [13] D.A.T.D. Rio Vaz, A.L. Amarante Mesquita, J.R.P. Vaz, C.J.C. Blanco, J.T. Pinho, An extension of the  
385 Blade Element Momentum method applied to Diffuser Augmented Wind Turbines. *Energy Convers Manage*  
386 2014; 87:1116–1123.
- 387 [14] L.B.Jr. Marshall, A new empirical relationship between thrust coefficient and induction factor for the  
388 turbulent windmill state. Technical report NREL/TP-500-36834, 2005.